High-Quality Electron Beams from Beam-Driven Plasma Accelerators by Wakefield-Induced Ionization Injection

A. Martinez de la Ossa,[1] J. Grebenyuk,[1] T. Mehrling,[1] L. Schaper,[2] and J. Osterhoff[1]

[1] *Deutsches Elektronen-Synchrotron DESY, D-22607 Hamburg, Germany*
[2] *Institut für Experimentalphysik, Universität Hamburg, D-22761 Hamburg, Germany*

(Dated: June 9, 2015)

We propose a new and simple strategy for controlled ionization-induced trapping of electrons in a beam-driven plasma accelerator. The presented method directly exploits electric wakefields to ionize electrons from a dopant gas and capture them into a well-defined volume of the accelerating and focusing wake phase, leading to high-quality witness-bunches. This injection principle is explained by example of three-dimensional particle-in-cell (PIC) calculations using the code OSIRIS. In these simulations a high-current-density electron-beam driver excites plasma waves in the blow-out regime inside a fully-ionized hydrogen plasma of density 5×10^{17} cm^{-3}. Within an embedded 100 μm long plasma column contaminated with neutral helium gas, the wakefields trigger ionization, trapping of a defined fraction of the released electrons, and subsequent acceleration. The hereby generated electron beam features a 1.5 kA peak current, 1.5 μm transverse normalized emittance, an uncorrelated energy spread of 0.3% on a GeV-energy scale, and few femtosecond bunch length.

PACS numbers: 52.40.Mj, 41.75.Ht, 52.25.Jm, 52.59.Bi, 52.59.-f

Over the last decade, the field of plasma-wakefield acceleration of electrons with ultra-high field gradients surpassing 10 GV/m has progressed steadily and rapidly. This is testified by the qualitative improvement of the accelerated beams during this period. In particular laser-driven wakefield accelerators [1] were improved significantly. Milestones, such as the realization of quasi-monoenergetic electron spectra [2–4], GeV-class beams [5], enhanced stability [6, 7], controlled injection techniques for tunability [8–10], and the application of the generated beams to drive compact XUV [11] and X-ray sources [12] promoted plasma-based acceleration to a promising technique for future accelerators.

Meanwhile, beam-driven plasma wakefield acceleration (PWFA) [13, 14] made great advancements, culminating in the demonstration of energy-doubling of part of the 42 GeV SLAC electron beam [15] in a distance of less than a meter. However, despite this remarkable progress, the quality of electron bunches extracted from beam-driven schemes lags behind those obtained from laser-driven plasma accelerators. This may mainly be attributed to the so far insufficient control over the electron-injection process in PWFA, which has a fundamental impact on the initial beam phase-space population and, thus, on the final beam quality.

Several controlled injection techniques for PWFA have been proposed but have not been experimentally verified yet, such as the external injection of a tailored witness beam [16], magnetically induced injection [17], and laser-triggered ionization injection [18, 19]. All these methods demand several elements in the experiment to act in concert to achieve injection into the appropriate wake region, e.g. fs synchronization and μm alignment of a laser to the particle beam or the generation of an adequate witness beam and its matching into the plasma wakefield [20]. These measures can be technically challenging to implement and a source of instabilities and, hence, may hamper the generation of high-quality electron bunches.

An easier approach constitutes the injection of electrons in plasma by means of field-induced ionization of a dopant gas with appropriate ionization potential, e.g. helium (He). It was recently discovered that this process can be initiated by the radial electric field of the driving beam [21]. However, the lack of control over the event and its sensitivity on initial conditions of the driving beam micro-structure did not lead to the production of qualitatively interesting beams. In this work, we propose a new and straightforward strategy for controlling ionization injection of electrons into beam-driven plasma wakes, utilizing the wake electric fields only and, thus, providing improved beam quality. This technique exploits the difference in absolute electric-field strength in the blow-out regime [22–24] existing between the accelerating and decelerating regions within the first wakefield bucket to selectively ionize a small volume of a background dopant gas near the phase of maximum acceleration only. In this way the production of high-quality, ultra-short ($\sim$ fs), low-emittance ($\sim$ μm), multi-GeV-energy electron beams from a relatively simple experimental setup is made possible.

PWFA in the blow-out regime uses a relativistic charged particle beam, which is short compared to the plasma wavelength and of higher density than the background plasma. This driver beam expels plasma electrons from its high-density core, forming a co-propagating ion cavity. The electric fields in this cavity or bubble may exceed the cold non-relativistic wave-breaking field $E_0 = (mc^2/e)\, k_p$, where $k_p = \sqrt{n_0 e^2/\epsilon_0 mc^2}$ is the plasma wave number, n_0 the plasma particle density, ϵ_0 is the vacuum permittivity, c the speed of light, and m and e are the

electron mass and charge, respectively. Current accelerator facilities provide short (rms lengths of $10-50$ μm) and dense (currents of $1-25$ kA) electron beams which are suitable to operate wakefields in the blow-out regime with accelerating fields of ~ 100 GV/m in plasmas with densities on the order of 10^{17}cm^{-3}. The amplitude of these accelerating electric fields is sufficient for ionization of electrons from a high-ionization potential atomic species such as He, and their trapping into a well defined phase of the wake near the back of the ion cavity. The ionization process caused by static (or slowly varying) electric fields of a magnitude sufficient to significantly deform the atomic potential barrier of an atom can be described by a tunneling probability [25], and has been determined for a number of atomic species [26]. Writing the tunneling-ionization rate in an engineering formula yields [27]

$$W_{ADK}[\text{fs}^{-1}] \approx 1.52 \frac{4^{n^*}\xi_i[\text{eV}]}{n^*\Gamma(2n^*)} \left(20.5\frac{\xi_i^{3/2}[\text{eV}]}{E[\text{GV/m}]}\right)^{2n^*-1} \times \exp\left(-6.83\frac{\xi_i^{3/2}[\text{eV}]}{E[\text{GV/m}]}\right),$$

where $\xi_i[\text{eV}]$ is the potential energy of the bound electron, $n^* \approx 3.69\ \text{Z}/\xi_i^{1/2}[\text{eV}]$ is the effective principal quantum number, which depends on the ionization level Z, and $E[\text{GV/m}]$ is the magnitude of electric field acting on the atom. The electric field $E = E_{ion}$ for which the ionization rate becomes $W_{ADK} = 0.1$ fs^{-1} is in this work considered as the ionization threshold. In case of He $E_{ion}^{He} = 93$ GV/m is predicted for the tunneling of the outer electron ($Z = 1,\ \xi_i = 23.6$ eV), and for the inner one ($Z = 2,\ \xi_i = 54.4$ eV) $E_{ion}^{He^+} = 235$ GV/m applies. The dynamics of electrons released by the above mechanism at a certain position in the wake can be addressed considering the electromagnetic Hamiltonian of a single electron $\mathcal{H}(\vec{x},\vec{P},t) = \sqrt{(mc^2)^2 + c^2(\vec{P}+e\vec{A})^2} - e\Phi$, characterized by the potentials $\Phi(\vec{x},t)$ and $\vec{A}(\vec{x},t)$ and the generalized coordinates $\vec{x}$ and $\vec{P} = \vec{p} - e\vec{A}$, where $\vec{p}$ is the momentum of the electron. In the co-moving system of reference with $\zeta = z - v_{ph}t$ and v_{ph} the phase velocity of the wake, the electromagnetic potentials barely change over time compared to their variation with ζ. Therefore, the quasi-static approximation [28] holds and $\partial_t = -v_{ph}\partial_\zeta = -v_{ph}\partial_z$. In this case, provided that $\dot{\mathcal{H}} = \partial_t\mathcal{H} = -v_{ph}\partial_z\mathcal{H} = v_{ph}\dot{P}_z$, the quantity $\mathcal{K} \equiv \mathcal{H} - v_{ph}P_z = mc^2\gamma - v_{ph}p_z - e\Psi$ is a constant of motion [29]. Here, we have defined the potential $\Psi \equiv \Phi - v_{ph}A_z$ related to the electric and magnetic fields by $E_z = -\partial_z\Psi$ and $E_r - v_{ph}B_\phi = -\partial_r\Psi$, while γ is the Lorentz factor of the electron. Immediately after ionization, the electron has negligible energy and can be considered at rest, thus $\mathcal{K}_i = mc^2 - e\Psi_i$. This electron is trapped into the wake if it follows a phase-space trajectory such that its velocity v reaches the velocity of the wake v_{ph}. When this happens, $\mathcal{K}_f = mc^2/\gamma_{ph} - e\Psi_f$, and since $\mathcal{K}_f = \mathcal{K}_i$, a trapping condition in terms of the difference in potential between the initial Ψ_i and trapped Ψ_f positions is derived [21]:

$$\Delta\Psi \equiv \Psi_f - \Psi_i = -\frac{mc^2}{e}\left(1 - \frac{1}{\gamma_{ph}}\right) \qquad (1)$$

For ultra-relativistic drivers ($v_{ph} \to c$ and $\gamma_{ph} \to \infty$), Eq. (1) can be written as $\Delta\Psi = -mc^2/e$. The initial position of the ionized electron inside the wake determines Ψ_i, and consequently its final trapping position (if any) along the corresponding Ψ_f equipotential contour. The necessary trapping condition for electrons ionized inside the first wake period, ahead of the minimum of potential Ψ_{min} at the rear of the ion cavity, is given by $\Psi_i > \Psi_{min} + mc^2/e \equiv \Psi_t$. The volume of injection is thus determined by the intersection of the volume of ionization ($E_i > E_{ion}$) with the volume satisfying the trapping criterion ($\Psi_i > \Psi_t$). Generally, the field configuration in the blow-out regime of PWFA can enable simultaneous ionization and trapping in two regions within the first wave bucket [30]. One is located at the driver beam position, where the radial electric field induces ionization. This ionization region is sensitive to the oscillating behavior of the beam in the focusing ion-plasma column [31] and fluctuations in the micro structure of its density profile. The second region of ionization is located at the rear of the cavity, where the wakefields induce ionization. In contrast to the front, the fields at the back are stable in time and barely dependent on details of the driver beam density profile and thus, provide a well-defined and controlled region for injection. The injection technique proposed in this work is designed to inject electrons only from a narrow phase interval at the back of the cavity, while preventing any contribution from the radial electric field of the driver.

To illustrate this method, we consider in the following electron bunches similar to those provided by the FACET facility at SLAC. These beams are approximated by Gaussian longitudinal ($\sigma_z = 14$ μm) and transverse ($\sigma_x = \sigma_y = 10$ μm) profiles with peak currents of 23 kA, transverse normalized emittances of $\epsilon_x = 50$ μm and $\epsilon_y = 5$ μm, and an energy of 23 GeV with a relative spread of 1 % [16]. The characteristics of these beams make them suitable to operate in the blow-out regime using a plasma with density $n_0 = 5\times10^{17}$ cm^{-3}, which can be generated using current gas cell technology [32]. As sketched in Fig. 1, a micro-nozzle [33] fed by a hydrogen-helium mixture with tunable ratio and pressure, is positioned in the vicinity of the gas cell entrance. The gas jet emerging from the nozzle is spatially confined to a diameter of about $L_{He} = 100$ μm, forming a highly localized region in which helium is present while not mixing with the gas cell volume, and overall maintaining a flat density distribution in line of sight of the electron

beam. In order to prevent an excessive beam loading, we choose a He concentration of $n_{He} = 0.002\ n_0$. In this setup, the plasma can be pre-created by means of a laser coaxial to the electron beam with an intensity $I_L \geq 1.52 \times 10^{14}$ W/cm^2 capable to fully ionize the hydrogen, but not the helium at $I_L \ll 1.14 \times 10^{15}$ W/cm^2, where the limits for the laser intensities are calculated from $E_{ion}^{He} = 93$ GV/m and $E_{ion}^{H} = 34$ GV/m, the ionization thresholds for He and H respectively.

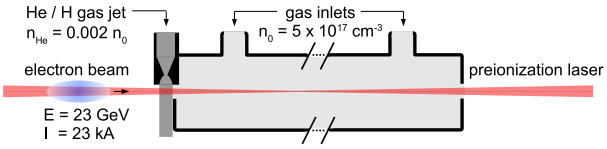

Figure 1. Schematic of the plasma-cell setup used in OSIRIS 3D simulations. A thin jet column of neutral H/He gas mixture is immersed in a laser pre-ionized hydrogen plasma at n_0.

Three-dimensional (3D) simulations of this setup have been performed using the particle-in-cell (PIC) code OSIRIS [34], which is capable of emulating ionization effects using the ADK model [26]. The moving window simulation box dimensions are $18 \times 30 \times 30\ k_p^{-3}$ with a cell size of $0.036 \times 0.060 \times 0.060\ k_p^{-3}$. Fig. 2(a) shows the electron density of the plasma (gray color palette), the driver beam (blue-yellow palette) and the ionized electrons (red-yellow palette) in the central slice (y vs. ζ, at $x = 0$) of the simulation inside the He region. The FACET beam drives accelerating wakefields which exhibit peak values greater than 200 GV/m (Fig. 2(b)). The magnitude of the electric field (Fig. 2(c)) in the accelerating region of the wake exceeds by far the threshold for the ionization of helium E_{ion}^{He}, whereas in the decelerating region of the wake it is significantly lower. To restrict the area of high ionization rate to the accelerating phase, the radial space charge field of the driver $|E_r|$, which is inversely dependent on the transverse beam size, must be less than E_{ion}^{He} during passage through the He gas jet. This can be ensured by placing the jet at the entrance of the plasma target, well before the beam experiments its first compression induced by the focusing ion-plasma cavity [31]. The length scale of transverse focusing of an unmatched beam is given by the betatron wavelength $\lambda_\beta = \sqrt{2\gamma}\ \lambda_p$ [35], in the considered case $\lambda_\beta \approx 14$ mm. Fig. 2(d) shows the probability of ionization $P_{ADK}(r, \zeta)$ of the He atoms streaming backwards with respect to the wake, obtained by integrating the ionization rate W_{ADK} in Eq. (1) along ζ. The contours where P_{ADK} reaches 10% and 100% of ionization are drawn in gray dotted and bold lines, respectively, defining a narrow phase interval $\{\zeta_{10}, \zeta_{100}\}$ extending up to the borders of the bubble, from which 90% of all possibly trapped He electrons

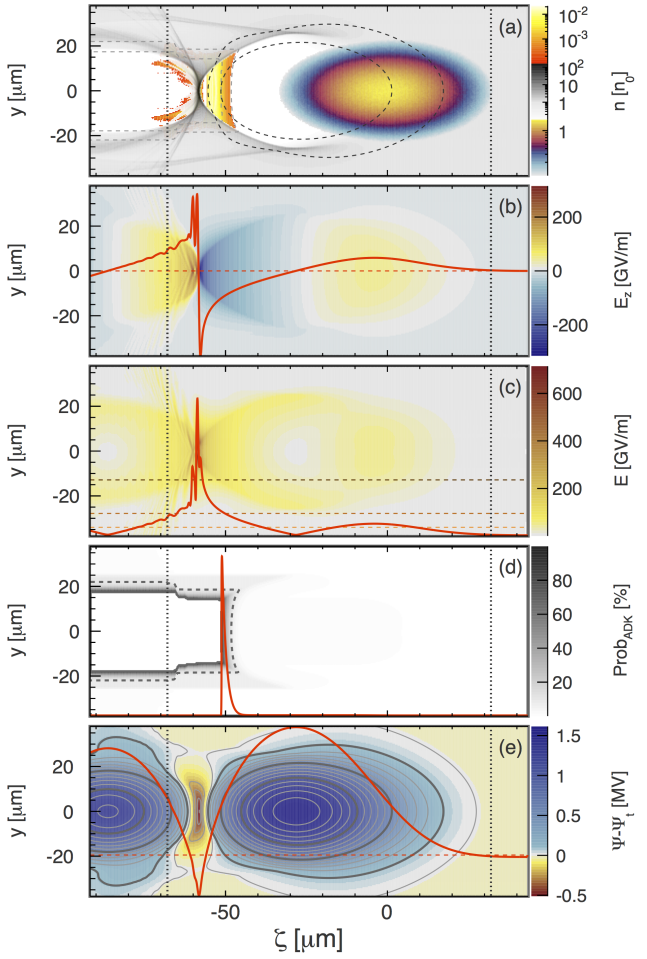

Figure 2. Central slices from a 3D OSIRIS simulation depicting the trapping conditions and showing ionization of electrons from a He dopant by wakefields excited by a FACET-type beam in a pre-created uniform plasma with a density of $n_e = 5 \times 10^{17}$ cm^{-3}. (a) Spatial particle density. Plasma (gray palette), driver beam (blue-yellow palette), and electrons ionized from He (red-yellow palette). (b) Longitudinal wakefields (blue-red palette) and on-axis (red line). (c) Total electric field (red palette) and on-axis values (red line). Light (dark) dotted red line shows the ionization threshold of the outer (inner) He electron. (d) ADK ionization probability of the first level of He (gray palette), the contour at 10 % probability (dotted line), and the on-axis values (red line). (e) The electric potential $\Psi - \Psi_t$ (blue-red palette), its contours in steps of $\Delta\Psi = 0.2 \times (mc^2/e)$, and the on-axis values (red line). Vertical dotted lines show the limits of the He column.

will be emerging ($\Delta\zeta_{ion} \equiv \zeta_{10} - \zeta_{100} \approx 3\ \mu$m). Fig. 2(e) depicts the trapping potential $\Psi - \Psi_t$, where positive values correspond to regions which allow trapping ($\Psi > \Psi_t$) and where equipotential contours are shown in steps of $0.2 \times mc^2/e$. The intersection of the volume with high ionization probability and the volume allowing trapping

yields the volume from which injected electrons can originate (Fig. 2(a)). However, trapping is also affected by the transverse dynamics of the electron in the plasma wave, i.e. by its initial radial position. Electrons released close to the boundary of the cavity may escape before the focusing force pushes them towards a stopping contour near the axis. A sufficient condition for trapping of an electron with a given initial radius is that it was trapped even if it kept the same radius when falling back with respect to the plasma wave, i.e. it reaches Ψ_f before the bubble boundary in straight backwards propagation. In this example, the maximum radius fulfilling the above condition is $R_{max} \approx 12$ μm (c.f. Fig. 2(a)). This allows for an estimation of the actual volume of injection $V_{inj} \simeq \pi R_{max}^2 \Delta\zeta_{ion}$ and hence for the total trapped charge $Q_{He} \simeq -en_{He}\, \pi R_{max}^2\, L_{He} = 7.2$ pC during passage through the He-doped gas column.

Fig. 3(a) shows a short (0.8 μm rms) bunch of electrons injected from the neutral He by means of the wakefields, in the above discussed simulation. With a total charge of 8.8 pC and a maximum peak current of 1.5 kA, the injected beam has been accelerating for 20 mm, positioned at $\langle\zeta_f\rangle = -55.7$ μm, where the longitudinal electric field is $E_z(\langle\zeta_f\rangle) \approx 130$ GV/m (Fig. 3(b)). Most physical properties of the trapped bunch can be estimated from the initial phase-space distribution. Trapped electrons with the same initial value of Ψ_i are positioned approximately on the same co-moving phase near axis during acceleration, fulfilling $\Psi_f(\zeta_f) = \Psi_i(\zeta_i) - mc^2/e$, and thus will be accelerated by the same field value $E_z(\zeta_f)$. However, each one of these slices in ζ_f is composed of electrons ionized at different longitudinal positions along the He column, and therefore accelerated at different times, producing a finite spread in longitudinal momentum in every slice given by $\Delta p_z(\zeta_f) \simeq -eE_z(\zeta_f)\, L_{He}$, which, at the average position of the bunch gives $\Delta p_z(\langle\zeta_f\rangle) \approx 13$ MeV. Moreover, the total relative energy spread is proportional to the variation of E_z along the bunch length, which in case of a negligible beam loading and sufficiently short bunches, is approximately given by $\Delta\gamma/\gamma \simeq \partial_\zeta E_z(\langle\zeta_f\rangle)/E_z(\langle\zeta_f\rangle)\, \Delta\zeta_f$. From Fig. 3(b), $\partial_\zeta E_z(\langle\zeta_f\rangle) \approx 10$ (GV/m) μm^{-1}, and $\Delta\gamma/\gamma \approx 6\%$. Electrons belonging to the same ζ_f slice come from different radial positions along their initial Ψ_i contour. Assuming full decoherence for every slice, an upper estimate of the uncorrelated normalized transverse emittance $\epsilon_y = \sqrt{\langle y^2\rangle\langle p_y^2\rangle - \langle y p_y\rangle^2}/mc$, can be given in terms of the initial transverse extend of the slice [30] $\epsilon_y = k_p\langle y_i^2\rangle/4$. Considering for simplicity, the largest Ψ_i contour to be uniformly distributed up to R_{max}, the estimated maximum sliced emittance yields $\epsilon_{y,max} = k_p R_{max}^2/12 \approx 1.4$ μm.

The properties of the simulated injected bunch after 20 mm of acceleration are summarized in Fig. 4. The longitudinal phase-space (Fig. 4(a)) exhibits linear chirp with an average energy of ~ 2.6 GeV and a total relative

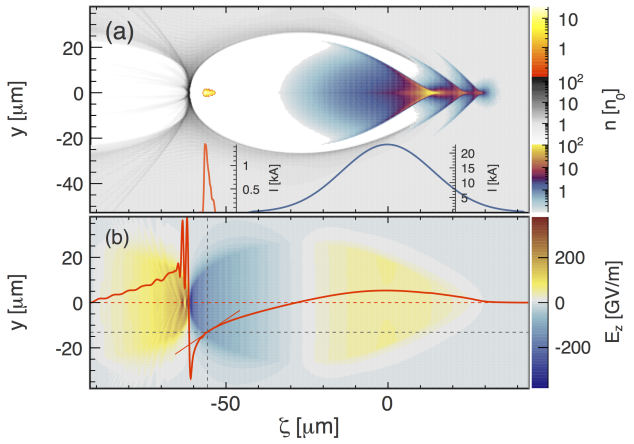

Figure 3. PIC simulation after 20 mm of beam propagation. (a) Charge densities of the electron plasma, beam and injected bunch. The curves show currents of the the drive beam (blue) and injected electrons (orange). (b) Longitudinal wakefields.

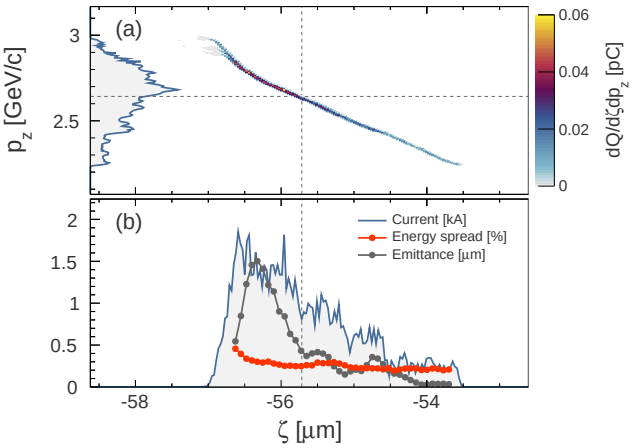

Figure 4. Witness bunch properties after 20 mm of acceleration. (a) shows the electron distribution of the bunch in longitudinal phase space (p_z vs. ζ plane). The projection of this distribution in p_z is depicted on the left axis. (b) displays the bunch current in dependence of the co-moving coordinate ζ. The relative energy spread (red points) and the transverse emittance (gray points) are plotted for different longitudinal slices along the bunch.

energy spread of 6%. The sliced bunch properties can be seen in more detail in Fig. 4(b). The current profile has a maximum at the tail of the bunch of ~ 1.5 kA and linearly decays towards its front (Fig. 4(b)). The relative energy spread ($\sim 0.3\%$), and the normalized transverse emittance (≤ 1.5 μm) are shown for different slices in ζ, demonstrating an excellent agreement with the analytical estimations given previously.

In summary, a new strategy for the injection of electrons in PWFA is proposed and demonstrated using 3D PIC simulations. The described method leads to a con-

trolled ionization-induced self-injection of electrons into blow-out plasma wakes in a simple experimental setup, which utilizes only the wakefields at the rear of the ion cavity to trigger the injection and trapping of electrons from a neutral atomic species into a well-defined phase of the plasma wake. As a result, high-quality electron bunches can be produced with short pulse lengths (≤ 1 μm), low normalized emittances (~ 1 μm), and low uncorrelated energy spread (< 1 %) on a GeV-energy scale. The first experiments demonstrating such beam quality will be regarded as important milestones in the ongoing endeavor to advance plasma-based particle accelerators for their future application in photon science and high-energy physics.

We thank the OSIRIS consortium (IST/UCLA) for access to the OSIRIS code. Special thanks for support go to J. Vieira and R. Fonseca. Furthermore, we acknowledge the grant of computing time by the Jülich Supercomputing Centre on JUQUEEN under Project No. HHH09. We would like to thank DESY IT for their support concerning simulations and data storage at DESY and the Humboldt Foundation for financial support.

[1] T. Tajima and J.M. Dawson, Phys.Rev.Lett. **43**, 267 (1979).
[2] S.P.D. Mangles *et al.*, Nature **431**, 535 (2004).
[3] C.G.R. Geddes *et al.*, Nature **431**, 538 (2004).
[4] J. Faure *et al.*, Nature **431**, 541 (2004).
[5] W.P. Leemans *et al.*, Nat. Phys. **2**, 696 (2006).
[6] J. Osterhoff *et al.*, Phys. Rev. Lett. **101**, 085002 (2008).
[7] N.A.M. Hafz *et al.*, Nat. Photon **2**, 571 (2008).
[8] J. Faure *et al.*, Nature **444**, 737 (2006).
[9] A. Pak *et al.*, Phys. Rev. Lett. **104**, 025003 (2010).
[10] A.J. Gonsalves *et al.*, Nat. Phys. **7**, 862 (2011).
[11] M. Fuchs *et al.*, Nat. Phys. **5**, 826 (2009).
[12] S. Kneip *et al.*, Nat. Phys. **6**, 980 (2010).
[13] V. Veksler, Proceedings of CERN Symposium on High Energy Accelerators and Pion Physics **1**, 80 (1956).
[14] P. Chen *et al.*, Phys. Rev. Lett. **54**, 693 (1985).
[15] I. Blumenfeld *et al.*, Nature **445**, 741 (2007).
[16] M. J. Hogan *et al.*, New Journal of Physics **12**, 055030 (2010).
[17] J. Vieira *et al.*, Phys. Rev. Lett. **106**, 225001 (2011).
[18] B. Hidding *et al.*, Phys. Rev. Lett. **108**, 035001 (2012).
[19] F. Li *et al.*, Phys. Rev. Lett. **111**, 015003 (2013).
[20] T. Mehrling, *et al.*, Phys. Rev. ST Accel. Beams **15**, 111303 (2012).
[21] E. Oz, *et al.*, Phys. Rev. Lett. **98**, 084801 (2007).
[22] J. Rosenzweig, *et al.*, Phys. Rev. **A44**, 6189 (1991).
[23] K. Lotov, Phys.Rev. **E69**, 046405 (2004).
[24] W. Lu, *et al.*, Phys. Rev. Lett. **96**, 165002 (2006).
[25] A. Perelomov, V. Popov, and M. Terentev, Sov. Phys. JETP **23**, 924 (1966).
[26] M. V. Ammosov, N. B. Delone, and V. Krainov, Sov. Phys. JETP **64**, 1191 (1986).
[27] D. L. Bruhwiler, *et al.*, Phys. Plasmas **10**, 2022 (2003).
[28] P. Sprangle, E. Esarey, and A. Ting, Phys. Rev. Lett. **64**, 2011 (1990).
[29] P. Mora and J. Thomas M. Antonsen, Phys. Plasmas **4**, 217 (1997).
[30] N. Kirby *et al.*, Phys. Rev. ST Accel. Beams **12**, 051302 (2009).
[31] C. E. Clayton *et al.*, Phys. Rev. Lett. **88**, 154801 (2002).
[32] C. E. Clayton *et al.*, Phys. Rev. Lett. **105**, 105003 (2010).
[33] P.-F. Hao *et al.*, Journal of Micromechanics and Microengineering **15**, 2069 (2005).
[34] R.A. Fonseca *et al.*, Lect. Notes Comput. Sci. **2331**, 342 (2002); R.A. Fonseca *et al.*, Plasma Phys. Control. Fusion **50**, 124034 (2008).
[35] E. Esarey *et al.*, Phys. Rev. **E65**, 056505 (2002).